Ultralow Reflection from *a*-Si Nanograss/Si Nanofrustum Double Layers

Srikanth Ravipati, Jiann Shieh, Fu-Hsiang Ko,* Chen-Chieh Yu, and Hsuen-Li Chen*

A requirement for any material to behave as a perfect optical absorber is that it absorbs all the light falling on it without any reflection.[1] A perfect optical absorber can improve the solar collection efficiency and, therefore, the overall solar-to-electricity efficiency.[2] To ensure high collection efficiency over an entire day, the perfect optical absorber must also be effective for all angles of light incidence (θ).[3] Many approaches have been developed to improve optical absorption. For example, a surface-modified NiP material has been reported to exhibit its lowest reflectance (R) of 0.16–0.18% at normal incidence,[4] but this reflectance increased at higher incident angles because of its micrometer-sized features and finite etch depth.[4a] Vertically aligned carbon nanotubes (VA-CNTs) have been employed recently to enhance the material darkness.[5a,b] Yang et al.[5a] reported the extremely low reflectance of VA-CNTs (R = 0.045%), measured using four different lasers operated at specific wavelengths in the visible light regime (457–633 nm). Unfortunately, very long VA-CNTs (ca. 800 μm) would be necessary to absorb all of the incoming light – an impractical requirement for solar cell applications. Another recent report described bottom-up single-crystalline Ni_xSi nanowires grown on low-cost flexible metal foil substrates over large areas, exhibiting excellent broadband anti-reflection properties (<1%) for visible and NIR wavelengths;[5c] unfortunately, the random orientations of these nanostructures obstructs their creation of p–n junctions when using current solar cell technology. Well-aligned nanostructures created using top-down approaches would be preferred over randomly oriented nanostructures when fabricating core/shell nanostructured solar cells. Another way to obtain ultralow reflection is to construct a profile featuring a graded refractive index on the surface. For example, SiO_2 and TiO_2 nanorod multilayers have been fabricated that exhibit an angle- and wavelength-averaged reflectance of 3.79%; this approach, however, requires a complex evaporation process, which is time-consuming and expensive, to prepare sequential layers of two materials with controlled porosity.[6] Silicon is another candidate for use in dark materials. According to simulations, the reflectance of VA-CNTs and pyramidal Si structures having the same period (10 nm) and height (2 μm) are 1.9 and 0.2%, respectively,[7] suggesting that sub-wavelength Si moth-eye structures are superior to VA-CNTs when used as antireflection materials. Silicon moth-eye structures, such as nanotips, can maintain their antireflection behavior over a broad range of wavelengths and angles.[8] Although very low specular reflectance has been reported for Si nanotips fabricated in a top-down manner,[8d] a large diameter is required to sustain the robustness of long nanotips, potentially increasing scattering during measurement of the reflection. For example, a diameter of 200 nm is required for 1.6 μm-long nanotips.[8d]

Recently, studies of double-layer nanostructures, including dual-diameter nanopillar structures[9a] and nanoisland-on-nanofrustum arrays,[9b] have demonstrated that such multiscale nanostructures exhibit performance – measured in terms of minimal reflectance and maximal absorption – superior to those of single-diameter nanopillars or sharp-tipped nanocone structures. Notably, when the light energy is larger than the band gap of *a*-Si, *a*-Si nanostructures are more effective at absorbing light – by nearly two orders of magnitude for a typical 1 μm-thick film – than are single-crystalline Si nanostructures.[10] Accordingly, we expected that a combination of *a*-Si and Si nanostructures of relatively short lengths would provide ultralow reflectance and higher absorption.

Herein, we demonstrate that unique double-layered nanostructures comprising amorphous silicon nanograss (*a*-Si NG) on top of silicon nanofrustums (Si NFs) behave as almost perfect optical absorbers. Our double-layered nanostructures were well aligned and had typical tip and base diameters of approximately 20 and 50 nm, respectively. The *a*-Si NG/Si NF structured materials exhibited ultralow reflectance and near-perfect optical absorption across a wide spectral range (300–800 nm); moreover, their responses toward transverse electric (TE) – and transverse magnetic (TM) – polarized incident light were almost indistinguishable over a wide range of angles of incidence (AOIs, from 20 to 60°), making them ideal optical absorber candidates for solar cell applications.

Tilt-view scanning electron microscopy (SEM) images of *a*-Si/Si nanostructures indicated that the average heights of the nanostructures increased upon increasing the etching time (**Figure 1**a–e). The density of the *a*-Si/Si nanostructure was less than that of single-crystalline Si nanograss.[11a–c] Because the stiffness of the *a*-Si thin films was much lower than those of Si or GaAs nanograsses,[11] longer etching periods resulted in spongy nanostructured *a*-Si films with lower packing density. The top-view

Dr. S. Ravipati, Prof. F.-H. Ko
Institute of Nanotechnology
Department of Materials Science and Engineering
National Chiao Tung University
Hsinchu 30010, Taiwan, ROC
E-mail: fhko@mail.nctu.edu.tw
Prof. J. Shieh
Department of Materials Science and Engineering
National United University
Miaoli 36003, Taiwan, ROC
E-mail: jshieh@nuu.edu.tw
C.-C. Yu, Prof. H.-L. Chen
Department of Materials Science and Engineering
National Taiwan University
Taipei 10617, Taiwan, ROC

DOI: 10.1002/adma.201204235

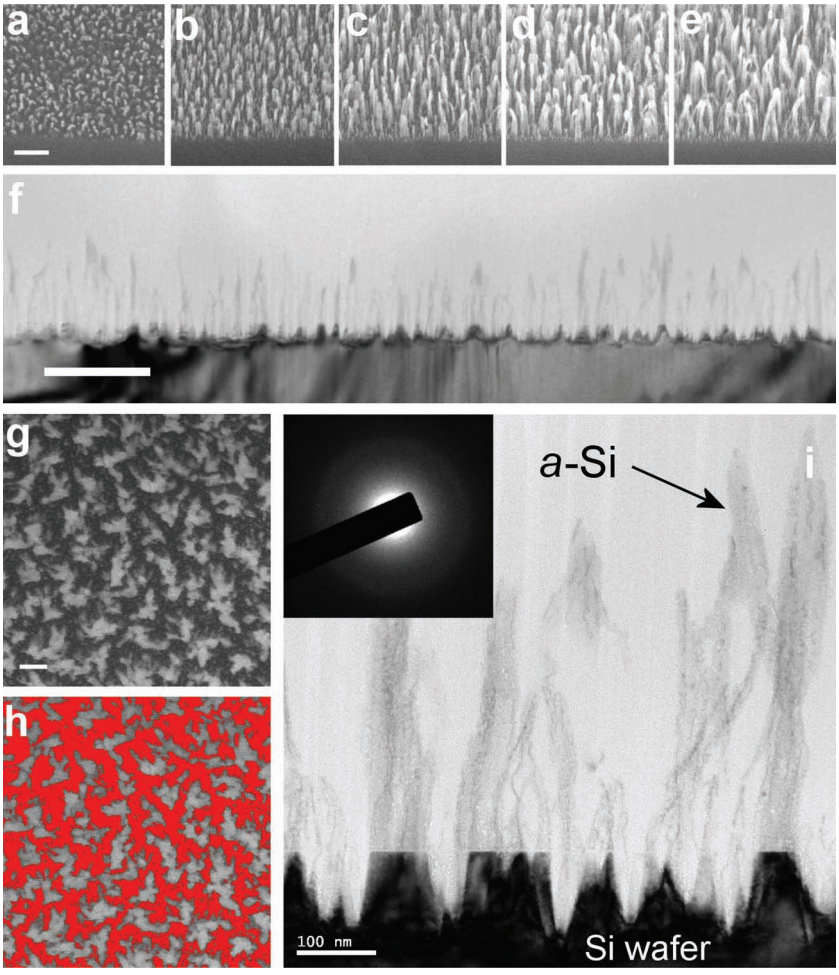

Figure 1. a–e) Tilt-view SEM images of *a*-Si/Si nanostructures etched for 10, 20, 30, 40, and 50 min, respectively (scale bar: 200 nm). f) Cross-sectional TEM images of the nanostructured sample etched for 90 min (scale bar: 200 nm). g) Top-view SEM image of the 90 min-etched sample, and h) corresponding contrast image used to estimate the filling ratio through imageJ analysis. i) Cross-sectional TEM images of the nanostructured sample etched for 90 min; inset: SAED pattern of the *a*-Si nanograss.

SEM images of the sample etched for 90 min in Figure 1g reveal that the density of the nanostructures was greater than 10^{10} cm^{-2}. We used the contrast difference in Figure 1h to calculate a surface filling factor (FF) of 45.4%, revealing that the packing density of amorphous Si nanograss was lower than that of single-crystal Si nanograss (>10^{11} cm^{-2}).[11b] To further analyze the *a*-Si/Si nanostructures, we recorded their transmission electron microscopy (TEM) images. Vertically aligned *a*-Si NG/Si NF structures were evident in the typical cross-sectional bright-field TEM image of the sample etched for 90 min (Figure 1f). Figure 1i displays an enlarged cross-sectional bright-field TEM image of the *a*-Si thin film sample etched for 90 min. The columnar nanostructure reveals that the etching proceeded through the *a*-Si thin film, reaching the *a*-Si–Si substrate interface, and continued to etch into the underlying single-crystal Si (100) substrate to form the Si NFs. The average tip and base diameters of these nanostructures were approximately 20 and 50 nm, respectively. We confirmed the presence of the *a*-Si structure on top of the NG layer from the diffuse ring of the selected area electron diffraction (SAED) pattern (inset to Figure 1i), which was recorded from the arrowed region in Figure 1i.

Figure 2a and 2b display the measured specular and total reflectances as a function of wavelength for *a*-Si NG/Si NF structures that had been etched for 30–120 min as well as for the *a*-Si thin film. The average specular and total reflectances of the *a*-Si thin film were 44.9 and 48.3%, respectively, over wavelengths from 300 to 800 nm. In contrast, all of the nanostructured samples exhibited reflectances (specular and total) that were significantly lower than those of the *a*-Si thin film over the entire spectral range, demonstrating their broadband antireflection characteristics. The ultralow reflectance observed for these nanostructured samples was presumably related to the smooth transition of the effective refractive index near the air–nanostructure interface.[8c,12a] According to the effective medium theory, the effective refractive index increases with the FF (the ratio of the area of the nanostructures to the total substrate surface area).[12] For the thinner nanostructured sample (170 nm), however, Fabry–Pérot oscillation of reflection amplitudes was still evident at longer wavelengths (Figure 2a), because shorter nanostructures with less variation in height can be regarded as smooth films.[12c] When light undergoes multiple reflections between two parallel surfaces (e.g., at air–nanostructure and nanostructure–Si interfaces), the multiple beams of light generally interfere with one another, resulting in oscillating reflection amplitudes. The average thicknesses of the *a*-Si thin film and the 30 min etched samples, calculated from the oscillation period, were 1177 and 693 nm, respectively (see Supporting Information). We observed that the interference patterns disappeared gradually with decreased reflectance upon increasing the length of the nanostructures. As a result, the sample of *a*-Si NG/Si NF structures etched for 120 min, with a feature height of 680 nm, had the lowest specular reflectance; indeed, the average specular and total reflectances were 0.10 and 0.34%, respectively, over the spectral range from 300 to 800 nm. These values are comparable with those previously reported for super-black materials[5a] and are two-orders of magnitude lower than that those of the 1 μm-thick *a*-Si thin film. Moreover, the features in our *a*-Si NG/Si NF structures are significantly shorter than those in previously reported CNT-based super-black materials, which required a feature height of 600–800 μm to obtain such low reflectance, highlighting the uniqueness of our system. Structures having lower-height features and, therefore, less-increased surface areas on near-zero–reflectance Si substrates are desirable for solar cell applications because the higher surface recombination caused by a larger surface area typically degrades the performance of a solar cell through

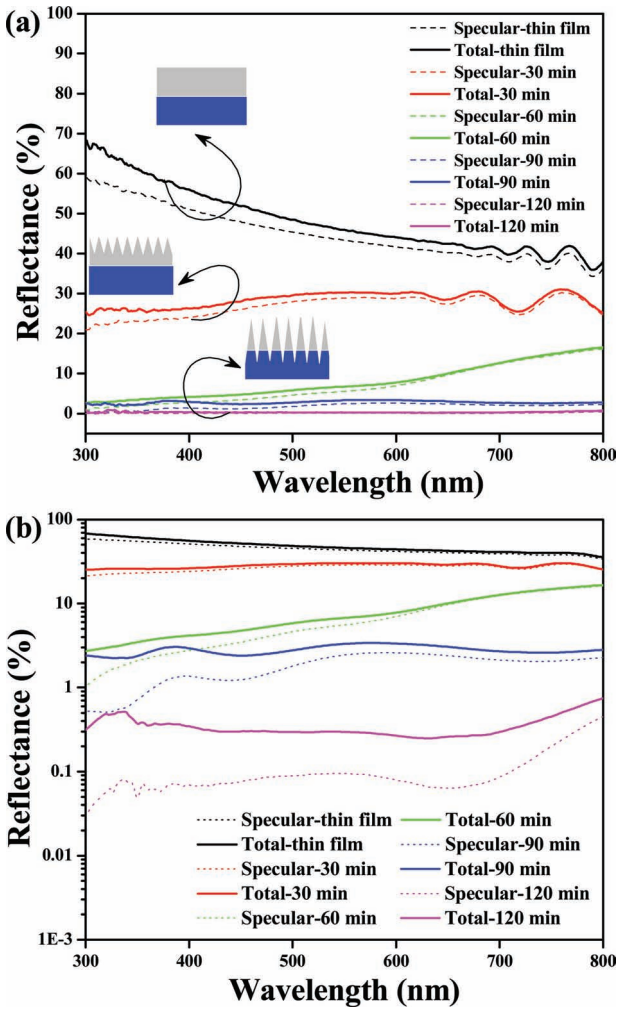

Figure 2. a) Measured specular (dashed lines) and total (thick lines) reflectances of *a*-Si/Si nanostructures; those of bare *a*-Si thin film (black curve) are also provided for comparison. b) The same reflectance data plotted on a logarithmic scale. The curves in (a) and (b) have been smoothed to decrease noise; the raw data are presented in Figure S1 in the Supporting Information.

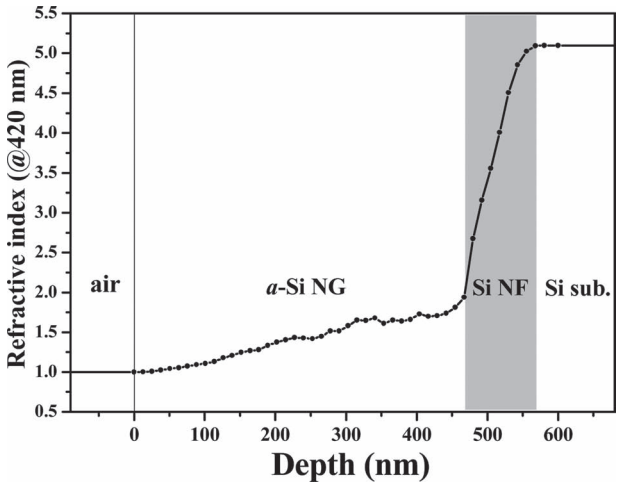

Figure 3. Refractive index profile of the 90 min-etched *a*-Si NG/Si NF structure, calculated from the cross-sectional TEM image in Figure S2 in the Supporting Information, with maximized contrast difference.

decreases in both the open circuit voltage and fill factor.[2a,2f,9b] Furthermore, the insignificant differences between the specular and total reflectances from the *a*-Si NG/Si NF structures reveals that the decrease in specular reflectance, due to light scattering, was small.[13] More importantly, the reflectance from the *a*-Si NG/Si NF structures was nearly wavelength-independent across a broad spectral range of wavelengths (300–800 nm).

To understand the cause of the near-zero reflectance, we calculated the refractive index profiles for the 565-nm-long *a*-Si NG/Si NF structures with 420 nm incident light. The effective refractive index (n_e) can be obtained using the weighting formula:[12d]

$$n_e(f) = f n_{Si} + (1 - f) n_{air} \quad (1)$$

where f is the FF of the nanostructures and n_{Si} and n_{air} are the refractive indices of Si materials[12e] and air, respectively. We divided the 565 nm-long *a*-Si NG/Si NF structure into 50 layers.

Figure 3 plots the calculated n_e profiles at 420 nm. For the calculations, we estimated the FF of the *a*-Si NG/Si NF structures from the cross-sectional TEM image with maximized contrast difference (Supporting Information, Figure S2). The gradient of n_e varied smoothly from 1 to 2 across the air–*a*-Si NG and *a*-Si NG–Si NF interfaces. At the air–*a*-Si NG interface, the refractive index of *a*-Si NG was close to 1 as a result of the surface roughness and low packing density of the *a*-Si structures, which allowed the incident light to enter into the materials without retardation from the change in refractive index. In addition, the transitions of the refractive index from 2 to 5.1 between the *a*-Si NG–Si NF and Si NF–Si substrate interfaces were also less abrupt, thereby also smoothing out the refractive index change between the *a*-Si structures and the Si substrate. Consequently, we believe that the smooth transition of the values of n_e, not only in the nanograss layer but also in the bottom NF layer, was the key to the ultralow reflectance, which was almost impossible to attain previously for super-dark materials[4,5] or other sub-wavelength single-layer moth-eye Si nanostructures with such short nanostructures.[8]

Conservation of energy requires all of the incident energy to be transmitted (T), reflected (R), and absorbed (A); that is, $T + R + A = 1$. Thus, a perfect optical absorber must satisfy the conditions $R \cong 0$, $T \cong 0$, and $A \cong 1$. We also measured the specular and transmittances over a broad range of wavelengths. Almost no transmittance occurred in the above-bandgap regime of *a*-Si for any of the nanostructured or thin film samples. The upper limit for the transmittance in our *a*-Si NG/Si NF structures at wavelengths from 300 to 800 nm was 0.06%. Therefore, the average total optical absorption of the 680-nm-high *a*-Si NG/Si NF structures in the spectral range from 300 to 800 nm, obtained from the expression $A = 1–R–T$, was 99.6%, (Supporting Information, Table S1) – that is, near-perfect optical absorption. The combination of near-perfect optical absorption and extremely low reflectance of these unique *a*-Si NG/Si NF structures over a broad range of wavelengths (from the UV to the near-IR) suggests that a greater proportion of solar energy might be

converted into electrical energy in solar cells, while maintaining a rather small thickness of the overall materials.[2g–i]

To investigate the effect of polarized light at larger AOIs, we performed specular reflectance measurements of double-layered *a*-Si NG/Si NF nanostructures (680 nm) at incident angles varying from 20 to 60° for both TE- and TM-polarized light (**Figure 4**a and 4b, respectively); reflectance measurements of the *a*-Si thin film are also presented for comparison. The reflectance of the *a*-Si thin film varied strongly with the AOI for both TE- and TM-polarized light. As the AOI increased from 20 to 60°, the reflectance of the *a*-Si thin film increased for all wavelengths (300–800 nm) – from 35.5% (20°, 792 nm) to 79.8% (60°, 300 nm) – for TE polarization; meanwhile, the TM reflectance decreased – from 57.0% (20°, 303 nm) to 11.2% (60°, 783 nm) – upon increasing the AOI from 20 to 60°. In contrast, the double-layered *a*-Si NG/Si NF nanostructures were insensitive to the polarization of light, with the reflectance remaining low and below 3.52% (60°, 304 nm) and 4.97% (60°, 318 nm) for TE- and TM-polarized light, respectively – considerably lower than that of surface-modified super-black NiP.[4a] At some specific wavelengths, the reflectance of the polarized light was as low as 0.01%. More importantly, the average reflectances (Supporting Information, Table S2) over all angles (20–60°) and all wavelengths (300–800 nm) were only 0.49% (TE) and 0.40% (TM); these values are comparable with those obtained for super-black CNTs[5a] and graded-refractive-index structures of SiO_2/TiO_2 multilayer nanorods.[6] These ultralow reflectances indicate that our unique double-layered *a*-Si NG/Si NF nanostructures are near-perfect optical absorbers that are almost insensitive to the polarization of light over a broad range of wavelengths and a wide range of AOIs.

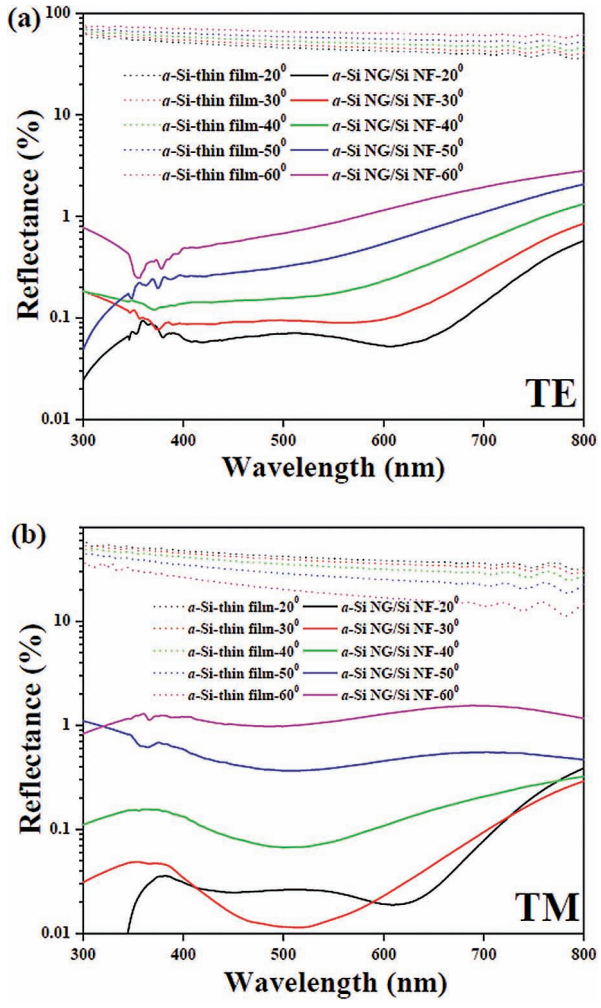

Figure 4. Specular reflectance data for the 680 nm *a*-Si NG/Si NF structured sample plotted on a logarithmic scale as a function of the AOI for TE-polarized (a) and TM-polarized (b) light over a broad range of wavelengths (from 300 to 800 nm). The reflectance of TE- and TM-polarized light from the *a*-Si thin film substrate is also presented for comparison. The curves in (a) and (b) have been smoothed to decrease noise; the raw data are presented in Figure S3 in the Supporting Information.

In summary, we have demonstrated a near-perfect optical absorber comprising thin (<680 nm), double-layered, sub-50 nm *a*-Si NG/Si NF nanostructures prepared using a simple, one-step, maskless plasma etching process. The average total absorption of our *a*-Si NG/Si NF structures was 99.6%, with an average total reflectance of 0.34%, at wavelengths between 300 and 800 nm. The measured angle- and wavelength-averaged reflectances of 0.49% (TE) and 0.40% (TM) reveal that the responses of these nanostructures to both types of polarization of light were almost indistinguishable over a broad range of wavelengths and a wide range of incident angles. The calculated refractive index profiles of the *a*-Si NG/Si NF structures revealed smooth transitions of the effective refractive index from the air to the Si substrate through both the *a*-Si nanograss and Si NF layers. We attribute the superior blackness of this near-perfect optical absorber to both the low density of its moth-eye-like nanograss profile and the presence of the NF transition underlayer. In addition, the degree through which the reflectance decreased through light scattering was insignificant, as evidenced by the inconsiderable difference between the specular and total reflectance. With their advantages of single-step fabrication, shorter nanostructures, and Si-based materials, our nanostructures appear to be efficient absorbers for use in thin-film solar cells. Such thin-film–based nanostructures might lead to the development of lower-cost, more-flexible devices as the crystal-Si substrate is replaced by other materials (e.g., polycrystalline Si or glass).

Experimental Section

Fabrication of a-Si NG on Si NF: To form *a*-Si/Si nanostructures, an undoped *a*-Si thin film having a film thickness of approximately 1 μm was first deposited at 625 °C on a 6 inch p-type Si (100) wafer (675 μm) through low pressure chemical vapor deposition (LPCVD). The as-deposited thin film, without undergoing any pre-cleaning process, was then loaded into the inductively coupled plasma chemical vapor deposition (ICPCVD) chamber. H_2 gas (165 sccm) was introduced and then the reactor pressure (30 mtorr) was maintained for plasma processing. A 13.56 MHz inductively coupled plasma (ICP) was used to dissociate H_2 gas and obtain a high density of hydrogen radicals, which bombarded the substrate to form the nanostructures. The morphologies and microstructures of the samples were analyzed using a scanning electron microscope (JEOL-JSM-6500F) and a transmission electron microscope (JEOL-JEM-2010F) equipped with an EDX analyzer.

Reflectance and Transmittance Measurements: The reflectance and transmittance measurements were performed using computer-controlled

equipment consisting of a collimated beam from a fiber-coupled tungsten-halogen and deuterium lamps at an interval of 1 nm; spectra were recorded using a Hitachi U-4100 various-angle optical spectrometer. The specular reflectance was measured at an incident angle of 5° with respect to the normal of the surface, while the transmittance was measured at normal incidence. For measurements of total reflectance, the samples were mounted at the backside of the integrating sphere at an angle of 10° with respect to the incident light beam. For measurements of transmittance, the samples were mounted in front of the integrating sphere. Measurements of the polarization-dependent reflectance (TE, TM) as a function of the wavelength and the AOI (20–60°) were measured using a polarizer (Hitachi); the sample was mounted in the inner stage and a power meter was positioned on the outer stage in a double-rotation stage (Hitachi).

Supporting Information

Supporting Information is available from the Wiley Online Library or from the author.

Acknowledgements

The nanofabrication process was performed at National Nano Device Laboratories (NDL). We thank H. M. Chen and F. J. Hou for technical assistance. Financial support was provided by the National Science Council of the Republic of China (contract NSC-100-2221-E-239-012-MY2).

Received: October 10, 2012
Revised: December 9, 2012
Published online: February 5, 2013

[1] R. A. Serway, *Physics for Scientists and Engineers with Modern Physics*, 2nd Ed., Saunders College Publishing, Philadelphia, PA USA **1986**.

[2] a) A. Cao, X. Zhang, X. Xu, B. Wei, D. Wu, *Sol. Energy Mater. Sol. Cells* **2002**, *70*, 481; b) A. R. Shashikala, A. K. Sharma, D. R. Bhandari, *Sol. Energy Mater. Sol. Cells* **2007**, *91*, 629; c) E. Garnett, P. Yang, *Nano Lett.* **2010**, *10*, 1082; d) J. Zhu, C. M. Hsu, Z. Yu, S. Fan, Y. Cui, *Nano Lett.* **2010**, *10*, 1979; e) V. Sivakov, G. Andra, A. Gawlik, A. Berger, J. Plentz, F. Falk, S. H. Christiansen, *Nano Lett.* **2009**, *9*, 1549; f) Y. R. Lu, A. Lal, *Nano Lett.* **2010**, *10*, 4651; g) M. D. Kelzenberg, D. B. Turner-Evans, M. C. Putnam, S. W. Boettcher, R. M. Briggs, J. Y. Baek, N. S. Lewis, H. A. Atwater, *Energy Environ. Sci.* **2011**, *4*, 866; h) S. W. Boettcher, J. M. Spurgeon, M. C. Putnam, E. L. Warren, D. B. Turner-Evans, M. D. Kelzenberg, J. R. Maiolo, H. A. Atwater, N. S. Lewis, *Science* **2010**, *327*, 185; i) M. D. Kelzenberg, S. W. Boettcher, J. A. Petykiewicz, D. B. Turner-Evans, M. C. Putnam, E. L. Warren, J. M. Spurgeon, R. M. Briggs, N. S. Lewis, *Nat. Mater.* **2010**, *9*, 239.

[3] H. A. Macleod, *Thin Film Optical Filters*, 3rd Ed., Taylor & Francis, London **2001**.

[4] a) R. J. C. Brown, P. J. Brewer, M. J. T. Milton, *J. Mater. Chem.* **2002**, *12*, 2749; b) The Darkest Manmade Substance, *Guinness World Records 2004*, Bantam Doubleday Dell Publishing Group, New York, May **2004**, p 242.

[5] a) Z. P. Yang, L. Ci, J. A. Bur, S. Y. Lin, P. M. Ajayan, *Nano Lett.* **2008**, *8*, 446; b) K. Mizuno, J. Ishii, H. Kishida, Y. Hayamizu, S. Yasuda, D. N. Futaba, M. Yumura, K. Hata, *Proc. Natl. Acad. Sci. USA* **2009**, *106*, 6044; c) N. P. Dasgupta, S. C. Xu, H. J. Jung, A. Iancu, R. Fasching, R. Sinclair, F. B. Prinz, *Adv. Funct. Mater.* **2012**, *22*, 3650.

[6] a) J. Q. Xi, M. F. Schubert, J. K. Kim, E. F. Schubert, M. Chen, S. Y. Lin, W. Liu, J. A. Smart, *Nat. Photonics* **2007**, *1*, 176; b) M. L. Kuo, D. J. Poxson, Y. S. Kim, F. W. Mont, J. K. Kim, E. F. Schubert, S. Y. Lin, *Opt. Lett.* **2008**, *33*, 2527.

[7] K. C. Hsieh, T. Y. Tsai, D. H. Wan, H. L. Chen, N. H. Tai, *ACS Nano* **2010**, *4*, 1327.

[8] a) Y. Kanamori, M. Sasaki, K. Hane, *Opt. Lett.* **1999**, *24*, 1422; b) C. Wu, C. H. Crouch, L. Zhao, J. E. Carey, R. Younkin, J. A. Levinson, E. Mazur, R. M. Farrell, P. Gothoskar, A. Karger, *Appl. Phys. Lett.* **2001**, *78*, 1850; c) C. Lee, S. Y. Bae, S. Mobasser, H. Manohara, *Nano Lett.* **2005**, *5*, 2438; d) Y. F. Huang, S. Chattopadhyay, Y. J. Jen, C. Y. Peng, T. A. Liu, Y. K. Hsu, C. L. Pan, H. C. Lo, C. H. Hsu, Y. H. Chang, C. S. Lee, K. H. Chen, L. C. Chen, *Nat. Nanotechnol.* **2007**, *2*, 770; e) L. Sainiemi, V. Jokinen, A. Shah, M. Shpak, S. Aura, P. Suvanto, S. Franssila, *Adv. Mater.* **2011**, *23*, 122.

[9] a) Z. Fan, R. Kapadia, P. W. Leu, X. Zhang, Y. L. Chueh, K. Takei, K. Yu, A. Jamshidi, A. A. Rathore, D. J. Ruebusch, M. Wu, A. Javey, *Nano Lett.* **2010**, *10*, 3823; b) H. Park, D. Shin, G. Kang, S. Baek, K. Kim, W. J. Padilla, *Adv. Mater.* **2011**, *23*, 5796.

[10] a) J. Zhu, Z. Yu, G. F. Burkhard, C. M. Hsu, S. T. Connor, Y. Xu, Q. Wang, M. McGehee, S. Fan, Y. Cui, *Nano Lett.* **2009**, *9*, 279; b) A. V. Shah, H. Schade, M. Vanecek, J. Meier, E. Vallat-Sauvain, N. Wyrsch, U. Kroll, C. Droz, J. Bailat, *Prog. Photovoltaics* **2004**, *12*, 113.

[11] a) M. C. Yang, J. Shieh, C. C. Hsu, T. C. Cheng, *Electrochem. Solid-State Lett.* **2005**, *8*, C131; b) J. Shieh, C. H. Lin, M. C. Yang, *J. Phys. D* **2007**, *40*, 2242; c) J. Shieh, F. J. Hou, Y. C. Chen, H. M. Chen, S. P. Yang, C. C. Cheng, H. L. Chen, *Adv. Mater.* **2010**, *22*, 597; d) S. Ravipati, J. Shieh, F. H. Ko, C. C. Yu, H. L. Chen, C. T. Wu, S. H. Chen, *Energy Environ. Sci.* **2012**, *5*, 7601; e) J. Shieh, S. Ravipati, F. H. Ko, K. Ostrikov, *J. Phys. D* **2011**, *44*, 174010.

[12] a) J. A. Dobrowolski, D. Poitras, P. Ma, H. Vakil, M. Acree, *Appl. Opt.* **2002**, *41*, 3075; b) D. A. G. Bruggeman, *Ann. Phys.* **1935**, *416*, 636; c) L. Hu, G. Chen, *Nano Lett.* **2007**, *7*, 3249; d) D. G. Stavenga, S. Foletti, G. Palasantzas, K. Arikawa, *Proc. R. Soc. London, Ser. B* **2006**, *273*, 661. e) E. D. Palik, *Handbook of Optical Constants of Solids*, Academic Press, OrlandoFLUSA **1985**.

[13] a) O. L. Muskens, J. G. Rivas, R. E. Algra, E. P. A. M. Bakkers, A. Lagendijk, *Nano Lett.* **2008**, *8*, 2638; b) Y. C. Chao, C. Y. Chen, C. A. Lin, J. H. He, *Energy Environ. Sci.* **2011**, *4*, 3436.